Pergamon

Acta Materialia 50 (2002) 4603–4616

Acta MATERIALIA

www.actamat-journals.com

An investigation of surface nanocrystallization mechanism in Fe induced by surface mechanical attrition treatment

N.R. Tao [a], Z.B. Wang [a], W.P. Tong [a], M.L. Sui [a], J. Lu [b], K. Lu [a,*]

[a] *Shenyang National Laboratory for Materials Science, Institute of Metal Research, Chinese Academy of Sciences, 72 Wenhua Road, Shenyang 110016, People's Republic of China*

[b] *LASMIS, University of Technology of Troyes, 10000 Troyes, France*

Received 10 April 2002; received in revised form 4 June 2002; accepted 18 July 2002

Abstract

By means of surface mechanical attrition (SMA), a nanostructured surface layer was formed on a pure Fe plate. Microstructure features of various sections in the surface layer, from the strain-free matrix to the treated top surface, were systematically characterized by using X-ray diffraction (XRD) analysis, scanning electron microscopy (SEM) and transmission electron microscopy (TEM) observations. Based on the experimental observations, a grain refinement mechanism induced by plastic deformation during the SMA treatment in Fe was proposed. It involves formation of dense dislocation walls (DDWs) and dislocation tangles (DTs) in original grains and in the refined cells (under further straining) as well, transformation of DDWs and DTs into subboundaries with small misorientations separating individual cells or subgrains, and evolution of subboundaries to highly misoriented grain boundaries. Experimental evidences and analysis of the grain refinement mechanism indicate that high strains with a high strain rate are necessary for formation of nanocrystallites during plastic deformation of metals.

Keywords: Nanocrystalline materials; Iron; Grain refinement; Microstructure

1. Introduction

Nanocrystalline (nc) materials, which are structurally characterized by nanometer-sized grains with a large number of grain boundaries, have been found to exhibit many novel properties relative to their coarse-grained counterparts [1,2]. For example, most nc metals and alloys possess high strength and hardness [3], as well as excellent tribological properties [4]. The workability of nc metals is much improved due to their enhanced superplasticity at lower temperatures compared to the conventional polycrystals [5,6]. These properties and performance enable nc materials to be potentially very useful in developing new material families with much enhanced properties for engineering applications and in upgrading the manufacturing process of traditional engineering materials in industries.

Nevertheless, research and development of bulk nc materials are hindered, to some extent, by various difficulties in synthesis techniques. Since the

* Corresponding author. Fax: +86-24-2399-8660.
E-mail address: lu@imr.ac.cn (K. Lu).

1359-6454/02/$22.00
PII: S1359-6454(02)00310-5

pioneering study of preparing bulk nc metals by means of gas condensation and consolidation by Gleiter et al., in the early 1980s, several processing techniques have been developed to produce bulk nc materials, e.g. consolidation of ultrafine powders prepared by various kinds of techniques [7], crystallization of amorphous precursors [8], ball-milling and consolidation [9], severe plastic deformation of bulk metals [10], and electrodeposition [11]. However, due to the limitation of each of these techniques, preparation of 'ideal' bulk nc samples (free of contamination and porosity, bulk in size, uniform and small (of a few nanometers) in grain size) is still a challenge to material scientists. Meanwhile much effort has been concentrated on improvement of these techniques for synthesizing bulk nc materials in recent years, the techniques for producing nanostructured surface layers are emerging quickly.

Most failures of materials occur on surfaces, including fatigue fracture, fretting fatigue, wear and corrosion etc., which are very sensitive to the structure and properties of the material surface. Optimization of the surface structure and properties may effectively enhance the global behavior of a material. As a result, the surface modification of engineering materials is found to process more and more industrial applications. With increasing evidences of novel properties in nc materials, it is reasonable to propose to achieve surface modification by the generation of a nanostructured surface layer so that the overall properties and behavior of the material are significantly improved. This kind of surface modification, referred as surface nanocrystallization (SNC), will greatly enhance the surface properties without changing the chemical composition [12]. It is also a flexible approach that makes it possible to meet specific structure/property requirements on surface of samples.

Nanostructured surface layers can be produced by means of various existing coating and deposition techniques such as PVD, CVD and plasma processing. Alternatively, SNC can be realized by means of grain refinement into the nanometer regime in the surface layer of a bulk material. Our previous investigations demonstrated that surface mechanical attrition (SMA) is an effective approach to create localized plastic deformation, resulting in grain refinement progressively down to the nanometer region in the surface layer of metallic materials [12–14]. The SMA process, which has been successfully applied in many material systems [15], has some unique advantages compared with the coating and deposition methods for SNC. For example, as there is no change in chemical compositions of the nc surface layer and in the matrix, as well as a gradient variation in the grain dimension from nano-sized (in the top layer) to coarse-grains (matrix), bonding of the nc surface layer with matrix will not be a problem. In addition, many existing mechanical processing techniques are applicable for synthesizing nanostructures in the surface by modifying the processing parameters, such as shot peening, hammer peening, surface rolling, laser shock processing, etc [12]. Therefore, this SNC approach has a great potential in industrial applications. For further development of the SMA technique, a clear understanding of the underlying mechanism for formation of nanostructures during the treatment is necessary. The objective of this work is to reveal the intrinsic mechanism for grain refinement during the SMA treatment in a pure iron sample.

Plastic deformation induced grain refinement has been known for many years [10,16]. Polycrystals with submicro-sized grains were usually fabricated via severe plastic deformation (SPD) of various metals and alloys by using equal-channel angular pressing (ECAP) [10], high pressure torsion [17] and cold rolling [18]. By examining the microstructure evolution in plastically deformed metals, possible grain refinement mechanisms were proposed, involving dislocation activities, formation of subgrain boundaries and grain boundaries [18,19]. The refinement process of coarse grains upon plastic deformation, in principle, depends on many intrinsic and extrinsic factors, such as structure and stacking fault energy of the material, the intensity of strains and strain rates, deformation temperature, and so on. Formation of nano-sized grains was realized in intensive mechanical attrition processes (such as ball-milling) in metals and alloys [20–22], in which much larger strains and strain rates were applied relative to the other SPD processes. In the milling process, fracture and

cold-welding of metal particles, as well as contamination from the milling media are involved, which make it difficult to identify the dominating mechanism for refining the grains into the nanometer scales. Therefore, up to now, a clear scenery of formation of nano-sized crystallites from coarse polycrystals by plastic deformation is still lacking.

In the SMA treatment, different microstructures can be obtained within the deformed surface layer along the depth from the treated surface to the strain-free matrix, i.e. from nano-sized grains to submicro-sized and micro-sized crystallites. This gradient structure results from a gradient change in applied strains and strain rates along the depth, from very large (top surface layer) to zero (strain-free matrix), in the treated surface layer. Obviously, the SMA treatment provides a unique opportunity to investigate the grain refinement mechanism by examining the microstructure features at different depths in the deformed surface layer, in which the deformation-induced evidences for grain refinement with different strains and strain rates are maintained.

2. Experimental

2.1. Sample

An iron plate ($70 \times 100 \times 100$ mm^{3}in size) with a purity of 99.95 wt%, was subjected to the SMA treatment in order to achieve a nc surface layer. Before SMA treatments, the plate surfaces were polished with silicon carbide papers and then annealed in vacuum at 1223 K for 120 min for diminishing the effect of mechanical processing and obtaining homogeneous coarse grains. The grain size of the annealed Fe plate is on average 100–150 μm.

2.2. SMA treatment [15]

Fig. 1(a) shows a schematic illustration of the SMA treatment set-up used in the present work. Stainless steel balls (shots) of 8 mm in diameter were placed at the bottom of a cylinder-shaped vacuum chamber that was vibrated by a generator, with which the shots were resonated. Because of the high vibration frequency of the system (50 Hz in this work, which can be varied up to 20 kHz [12,13]), the sample surface to be treated was peened by a large number of shots in a short period of time. Each peening of the ball to the surface will result in plastic deformation in the surface layer of the treated sample (as shown in Fig. 1(b)). As a consequence, repeated multidirectional peening at high strain rates onto the sample surface leads to severe plastic deformation in the surface layer. In this work, the samples were treated in vacuum for 60 min at room temperature. After the SMA treatment, the sample surface is smooth (with comparable roughness as the original polished sample). Positron annihilation spectroscopy experiments revealed that the surface layer of the SMA treated sample is free of porosity.

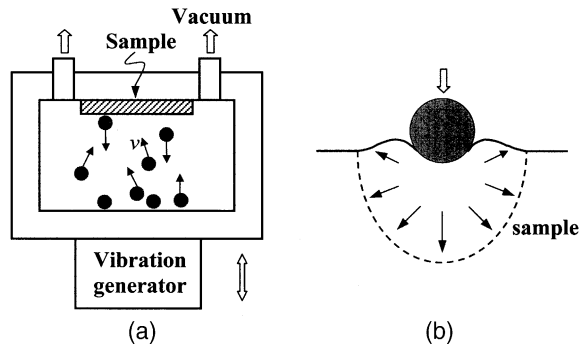

Fig. 1. Schematic illustrations of the SMA treatment set-up (a) and the localized plastic deformation in the surface layer by the impacting of the shot (b).

2.3. Microstructural characterization

X-ray diffraction (XRD) analysis of the surface layer in the SMA treated Fe sample was carried out on a Rigaku D/max 2400 X-ray diffractometer (12 kW), with Cu K_α radiation (wavelengths $\lambda_{K\alpha1} = 1.54056$Å and $\lambda_{K\alpha2} = 1.54439$Å were reflected by a graphite crystal using the (0002) reflection). Small angular steps of $2\theta = 0.02°$ were taken to measure the intensity of each Bragg diffraction peak. The counting time of 20 s was used to exactly measure the width of diffraction peak in the step-scanning mode. The average grain size and mean microstrain were calculated from line broadening of bcc Fe (110), (200), (211), (220),

(310) and (222) Bragg diffraction peaks, by using the Scherrer and Wilson method [23]. By using repeated electrochemical etching, the treated surface layer was removed layer-by-layer, so that the microstructural evolution along the depth from the treated surface was determined by means of XRD analyses.

Cross-sectional observations of the treated Fe sample were preformed on a JSM-6301F scanning electron microscope (SEM). Microstructure features in the surface layer were characterized by using a Philip EM-420 transmission electron microscope (TEM, operating at a voltage of 120 kV) and a JEOL-2010 high-resolution electron microscope (HREM, at 200 kV), respectively. Plane-view and cross-sectional thin foils for TEM and HREM observations were prepared by means of cutting, grinding, dimpling and a final ion thinning at low temperatures.

3. Results

3.1. Variation of grain size along depth

Fig. 2 is a cross-sectional SEM observation of the SMA treated Fe sample. Obviously, microstructure morphology of the treated surface layer (of about 60 μm thick) differs from that in the matrix. Severe plastic deformation evidences are seen in the surface layer, in which grain boundaries could not be identified as in the matrix. It is noted that the surface deformation layer thickness in the entire Fe plate surface is not uniform from place to place (±20 μm), indicating the heterogeneity of plastic deformation induced by the repeated peening. This may be attributed to the heterogeneous nature of the plastic deformation both within and between grains [24].

XRD analyses were carried out for determining the average grain (or cell) size and the microstrain in the surface layer. With consideration of the Cu K_α wavelength and its extinction depth in Fe, XRD patterns reflect the structure information from the surface layer of about 5 μm thick. By removal of the surface layer-by-layer, structure evolution along the depth can be determined. For the top surface layer, evident broadening of Bragg diffraction

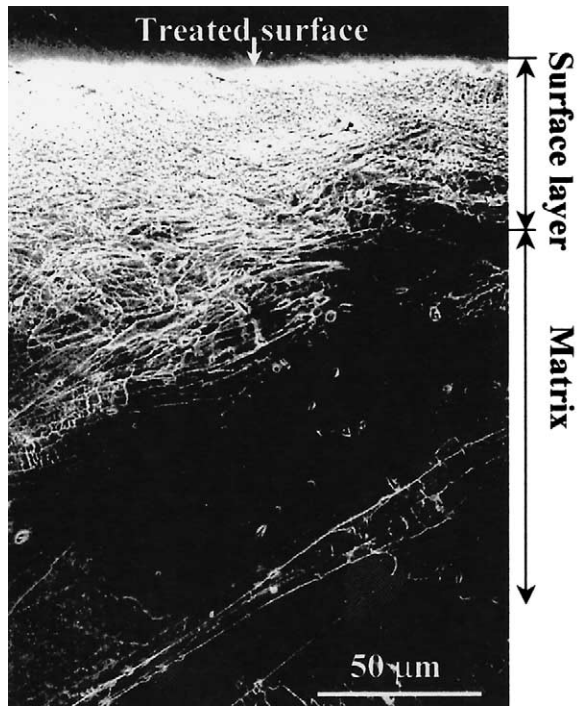

Fig. 2. A cross-sectional SEM observation of the SMA treated Fe sample for 60 min.

peaks was seen owing to a grain refinement and an increase in the atomic-level microstrain. The average grain size was calculated to be about 12 nm and the mean microstrain is 0.12%. These values are comparable to those for the ball-milled Fe powder sample reported [25]. It implies a similar processing intensity between the SMA treatment (in the top surface layer) and the ball-milling process.

The XRD peak broadening becomes less evident as the depth increases, indicating that grain sizes gradually increase and/or the microstrain decreases. When the grain size is larger than 100 nm, the XRD analysis results become inaccurate due to the large uncertainty in measuring the peak broadening. TEM and SEM observations were employed to determine the grain size. Fig. 3 shows a typical TEM plane-view observation of the top surface layer (about 1 μm deep) in the SMA treated Fe sample. It is clear that the microstructure is characterized by ultrafine equiaxed grains (bcc Fe) with random crystallographic orientations, as indi-

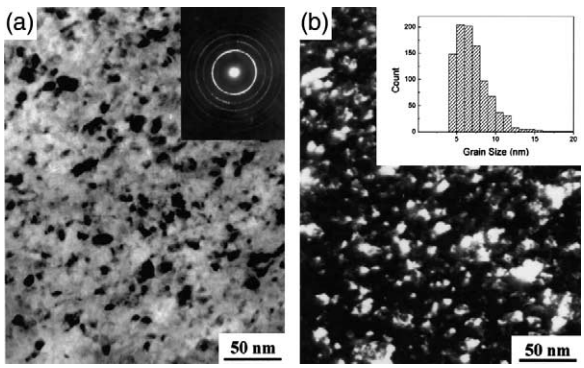

Fig. 3. (a) Bright-field and (b) dark-field TEM images showing planar microstructures of the top surface layer in the SMA treated Fe sample (insert is a statistic distribution of grain size derived from the dark-field TEM images).

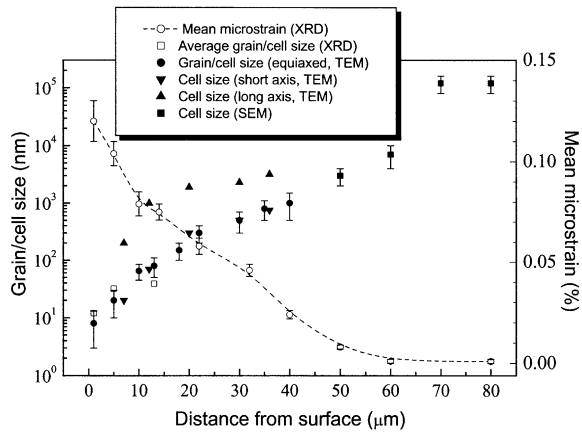

Fig. 4. Variations of the grain/cell size and the mean microstrain with the depth from the treated surface of the Fe sample determined by means of XRD analysis, TEM and SEM observations. In TEM observations, sizes of the equiaxed cells and the lamellar cells (along short axis and long axis) are measured.

cated by the selected area electron diffraction (SAED) pattern. The histogram of grain size distribution obtained from the dark-field images was characterized by a normal logarithmic distribution with a narrow size distribution (insert). The mean grain size is approximately 7 nm, which is slightly smaller than the XRD result (12 nm). This might be partially attributed to the fact that the XRD result averages the structure information of the top surface layer of about 5 μm thick. All diffraction rings in the SAED pattern were identified as bcc Fe, and no other phases were detected.

The microstrain determined from XRD analysis decreases significantly along the depth in the surface layer and gradually drops to zero at about 60 μm deep. From cross-sectional TEM and SEM observations, we noticed evidences of dislocation activities induced by the attrition treatment in even deeper matrix (up to 110 μm deep), where no change in grain size and atomic-level microstrain is detected. The measured average grain (or cell) size and the mean microstrain as a function of depth in the SMA treated Fe sample by using different analysis techniques (XRD, SEM, and TEM) are summarized in Fig. 4. In terms of the grain (or cell) size, the SMA treated surface layer can be subdivided into four sections along depth from the top surface:

section (i): nanostructured regime (0–15 μm);
section (ii): submicro-sized regime (15–40 μm);
section (iii): micro-sized regime (40–60 μm);
section (iv): matrix with plastic deformation evidences (60–110 μm).

3.2. Microstructure features

The experimental results clearly demonstrated that nanostructures developed in the surface layer of the Fe plate during the treatment. In order to understand the microstructure evolution process in the surface layer during the treatment, a systematic investigation on the microstructure in the surface layer at different stages of straining is needed. As the straining decreases from maximum at the top surface layer to zero in the matrix, the structure evolution process during the SMA treatment may be signed by the microstructure characteristics (with different strains) at different depths from the top surface to deep matrix. Therefore, detailed cross-sectional TEM observations were performed on the treated Fe sample.

3.2.1. Dislocations, dense dislocation wall and dislocation tangle

Fig. 5 shows TEM observations in the deformation layer at low strains adjacent to the strain-free matrix (60–80 μm deep from the top surface,

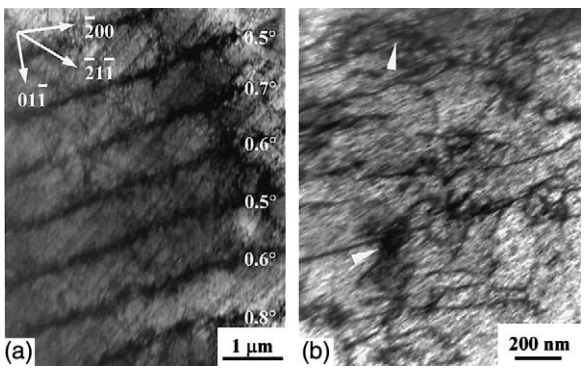

Fig. 5. Cross-sectional TEM images in the matrix of the treated sample with plastic deformation evidences of DDWs ((a) numbers signifying misorientations across DDWs), and DTs ((b) in which white arrows indicate location of high dislocation density regimes).

section (iv)), in which three typical deformation-induced microstructure features were identified:

1. Dislocation lines (DLs): Homogeneously distributed DLs are observed in Fe {110} planes and other sliding planes (such as {112} and {123}), depending upon the orientations of the grains. The density of DLs increases with a decrease of depth from the top surface.
2. Dense dislocation walls (DDWs): They are frequently seen inside some grains in this section, as shown in Fig. 5(a). These DDWs (along Fe {110} planes) are parallel to each other separated with a uniform spacing. It is noticed that the spacing between parallel DDWs varies (from a fraction of micron to a few microns) from grain to grain, depending upon grain orientations. DDWs are believed to result from dislocation accumulation and rearrangement for minimizing the total energy state. It is worth noting that small misorientations across DDWs are detected, usually smaller than 1° (as indicated in Fig. 5(a)). Meanwhile, dislocation lines along the {112} planes are also visible, which intersect with DDWs in the {110} planes. Intersecting DDWs are occasionally observed in some grains in which DDWs were developed simultaneously in different slip planes.
3. Dislocation tangles (DTs): In some grains, the dislocation distribution is not uniform and in some regions the dislocation density is rather high. High-density dislocations arraying in tangles were observed, as in Fig. 5(b). In tangles dislocations are randomly arranged without preferable sliding orientations.

3.2.2. Grain subdivision and subgrains

As the depth decreases, deformation strains and strain rate increase. In the micro-sized regime (section (iii), 40–60 μm deep), most original grains are found to be subdivided into micro-sized cells (or 'blocks'), of which the shapes are either roughly equiaxed or lamellar in cross-sectional TEM observations.

Fig. 6 shows these regular-shaped (parallelogram) cells separated by two sets of intersecting DDWs in the {110} planes. These intersecting DDWs seem to 'cut' the original coarse grain into refined (micro-sized) blocks, across which small misorientations (less than 1°) are observed.

Fig. 6. A TEM image showing intersecting DDWs developed in two sets of {110} planes that cut the original grain into parallelogram cells.

Fig. 7 shows lamellar-shaped cell structures with a width of about 400–1000 nm and a length of about a few microns (section (ii)). Similar lamellar-shaped structures were also observed in tension experiments of Fe [26,27]. The lamellar cells are separated by evident 'boundaries' in the long axis (along the {110} planes). These 'boundaries' are obviously sharper and thinner than the DDWs (as in Fig. 6), and the misorientations across them are much larger (usually a few degrees) than those for DDWs. It is reasonable to believe these 'boundaries' (referred as 'subboundaries') are developed from original DDWs by accumulation and annihilation of more dislocations. By absorbing of more and more dislocations, the DDWs may transform into subboundaries (i.e. small-angle grain boundaries) with an increased misorientations. In Fig. 7, some parts of DDWs along the long axis have not been transformed completely into the subboundaries, as indicated. DDWs along the short axis of the cells are also observed to be along the {110} planes, which intersect the subboundaries along the long axis. Misorientations across adjacent DDWs were observed to be less than 1°. Some intersecting DDWs are tilted probably due to the mutual interaction with dislocations.

The intersection of DDWs along the short axis with subboundaries (long axis) results in further refinement of the cells by 'cutting' the lamellar cells into smaller cells. By accumulating more dislocations with further straining, the 'cutting' DDWs may become subboundaries with larger misorientations. As seen in Fig. 7, intersecting DDWs and subboundaries can form a parallelogram structure. With the transformation of DDWs (along the {110} planes) into subboundaries with large misorientations, roughly equiaxed cells surrounded by subboundaries are formed (see the cell labeled by 'X').

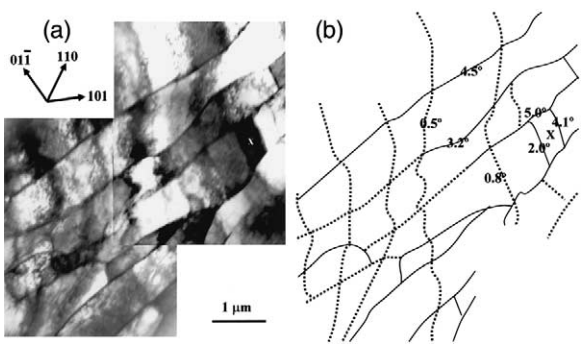

Fig. 7. Cross-sectional TEM images at 37 μm deep from the top surface of the Fe sample. Submicro-sized lamellar cells separated by DDWs (dotted lines) and subboundaries (solid lines) are seen. Numbers indicate misorientations across adjacent cells.

With an increase of strain at smaller depth, the number of DDWs and subboundaries increases, and intersections of DDWs and subboundaries appear more frequently, so that smaller cells were observed. Fig. 8 shows the cross-sectional microstructures observed at the depth of about 24 μm from the top surface. The microstructures are characterized by lamellar cells and subgrains, of which the sizes are evidently smaller than those in Fig. 7. The size of lamellar cells along the long axis ranges from about one to several micrometers, and the short axis size is about 200–400 nm. Similar to Fig. 7, the submicro-sized lamellar cells are separated by either DDWs or subboundaries. Cells 2 and 3 along the short axis as well as cells 2 and 4 along the long axis are separated by DDWs, which have not yet been transformed into subboundaries. Subboundaries were found between cells 3/4, 4/5 and 5/6. Development of some subboundaries from the DDWs is seen in progress, e.g. between cells 4/5 and 5/6, as indicated in Fig. 8.

It is noticed that these cells can be further divided into smaller lamellar or equiaxed substructures via development of more DDWs and subboundaries. As one can see in cell 1 in Fig. 8, development of new DDWs parallel to the long axis is in progress (as indicated), which may eventually result in formation of subboundaries, leading to subdivision of the cell. Formation of DDWs in other directions inside a cell is also possible, for example, in cell 6. DDWs normal to the long axis of cell 5/6 subboundary are formed, which may cut the cell into more cells with small length/thickness ratios. High density dislocations exist in some cells (as seen in cell 6), which can probably be subdivided by development of DT structures and subboundaries, as will be discussed in the following section.

Another typical microstructure observed in the submicro-sized regime is characterized by equi-

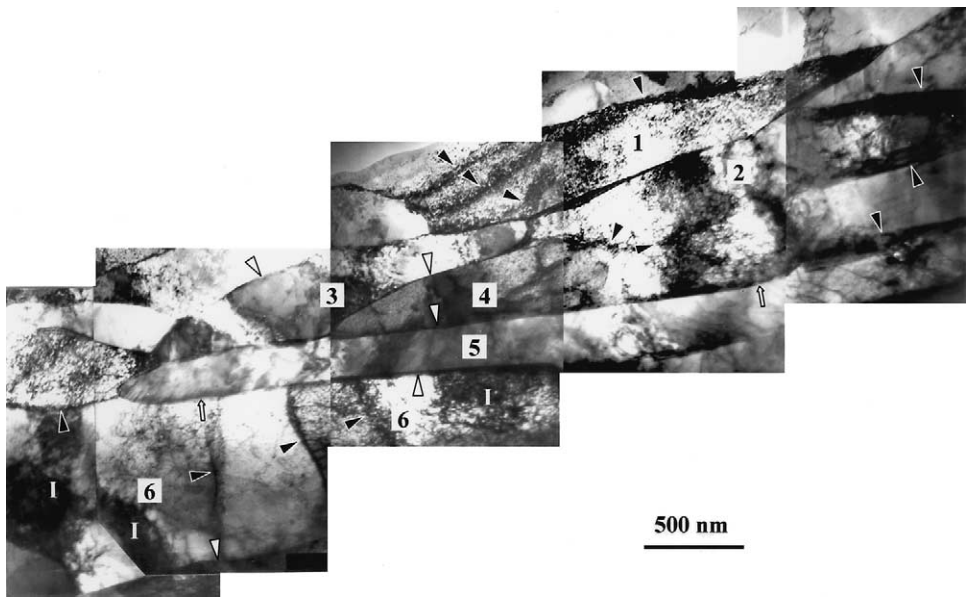

Fig. 8. A cross-sectional TEM image in the submicro-sized section (24 μm deep from the top surface) showing lamellar dislocation cells and subgrains with different dislocation configurations and boundaries (solid triangles for DDWs, open triangles for subboundaries, arrows for undeveloped subboundaries and letters I for location of high dislocation density regimes).

axed cells (or subgrains), as shown in Fig. 9. The size of cells is about 200–500 nm, and small misorientations were detected among these cells. As in the lamellar-shaped cells, the equiaxed cells are also separated by DDWs, DTs, or subboundaries, as can be clearly seen in Fig. 9. It is noticed that the subboundaries of the equiaxed cells have not specific orientations (in the lamellar cells, the subboundaries are normally parallel to the slip planes). One may speculate that these subboundaries are developed from the high-density DTs in which no preferable orientation exists. Development of DTs into subboundaries can be seen in Fig. 9, as indicated. The wide 'band' of DTs (indicated by solid arrows) seem to form a new subboundary. Inside some cells one can see evident contrasts of a high density of lattice dislocations, which may involve in further refinement of the cells with increasing strains. Eventually, those subboundaries transform into conventional grain boundaries with large misorientations by accumulating more dislocations, and orientations of the grains become random. Fig. 10 shows equiaxed grains with sizes of about 300 nm observed at the depth of about 28 μm from the top surface. These grains with random orientations (as evidenced by SAED pattern) are separated by sharp conventional boundaries. Also, dislocations inside the grains are present, as in typical microstructure developed by severe plastic deformation [28].

3.2.3. Nanostructures

The deformation strain and strain rate are drastically increased in the top surface layer. Nano-sized microstructures were observed in the regime of from 15 μm deep to the top surface. Close to the top surface, nano-sized equiaxed nanocrystallites are seen, and lamellar-shaped nanograins are present at the bottom of this section (adjacent to the submicro-sized section). Figs. 11 and 12 show typical cross-sectional observations of the microstructure in this section. In Fig. 11(a), lamellar grains of 10–50 nm thick and 50–100 nm long are observed. It is worth noting that inside the inner of these lamellar nanocrystallites, there exist even smaller equiaxed nano-grains. In Fig. 11(b), one can see roughly equiaxed nanocrystallites with sizes of about 30 nm. The SAED pattern indicates small misorientations among these nanocrystallites. Evidently, these equiaxed nanograins were

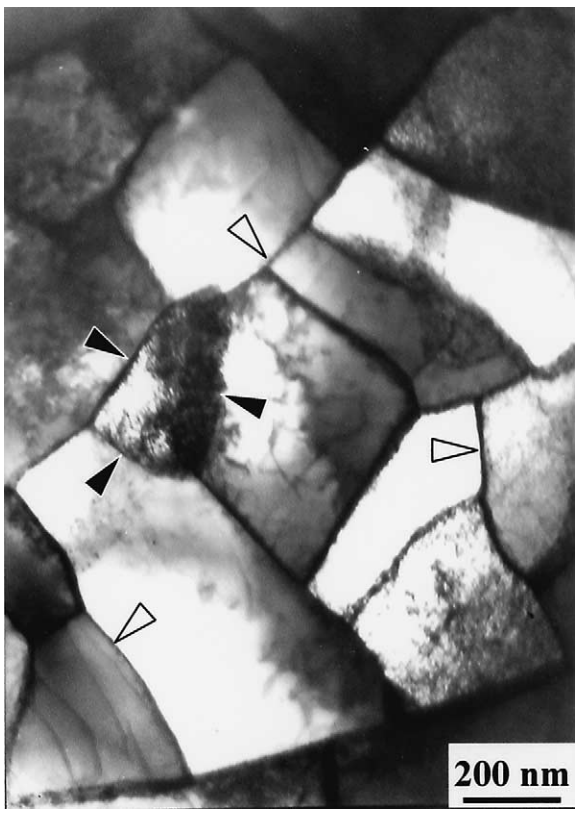

Fig. 9. A cross-sectional TEM image in the submicro-sized section showing equiaxed subgrains with different dislocation configurations and boundaries (solid triangles for DDWs and DTs, open triangles for subboundaries).

formed by breaking up the nano-sized lamellar grains (or cells) due to dislocation accumulation and subboundary development, as in the case of submicro-sized section. Misorientations between the neighboring nanocrystallites gradually increase to large angles with further straining. Then, equiaxed nanocrystallites with random orientations can be achieved. Fig. 12 shows a cross-sectional TEM observation at the very top surface layer. One may see equiaxed nanocrystallites of about 10–20 nm in size, and their crystallographic orientations are random, as indicated by the SAED pattern. From the dark-field TEM image in Fig. 12, it is interesting to find that the nanocrystallites seem to be arranged in parallel arrays. The nanocrystallite arrays seem to be formed by cutting nano-sized lamellar cells by means of development of more

Fig. 10. A cross-sectional TEM image in the submicro-sized section (28 μm deep) showing equiaxed grains separated by large misorientaion boundaries.

boundaries along the short axis. The random orientations of the nanocrystallites may be resulted from formation of high-angle grain boundary and/or grain rotation under large strains.

A close observation of the nanostructure in the top surface layer was performed by using HRTEM, as depicted in Fig. 13. The nano-sized crystallites with different misorientations were clearly identified, including large angles (nanocrystallites a and b) and small ones (nanocrystallites c and d, about 5°). From the plane-view (Fig. 3 and Fig. 13) and the cross-sectional view (Fig. 12) of the top surface layer, one may conclude that equixed nano-sized grains are formed in the top surface layer in the Fe sample.

4. Discussion

Microstructural investigations revealed that ultrafine-grained structures (from nano- to micro-

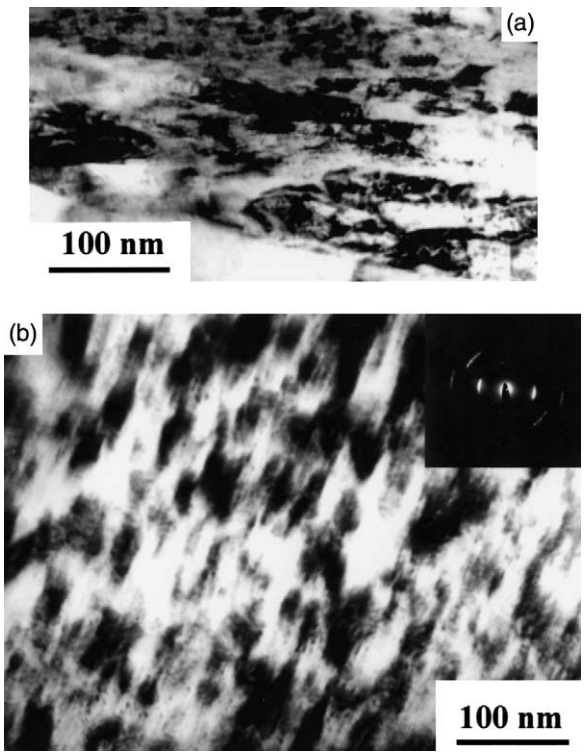

Fig. 11. Cross-sectional TEM images in the top surface layer showing: (a) lamellar nanocrystallites; (b) equiaxed nanocrystallites with small angle misorientations.

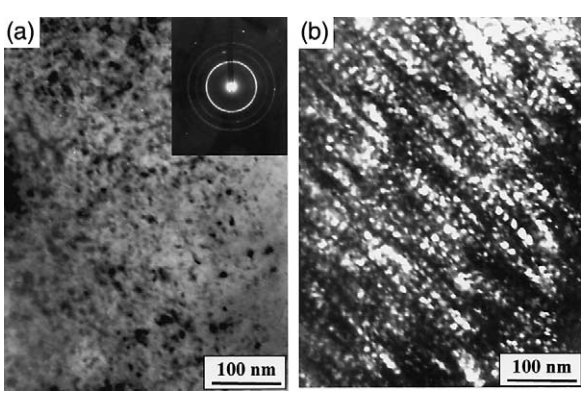

Fig. 12. (a) A bright-field and (b) a dark-field cross-sectional TEM images showing nanocrystallites in the very top surface layer.

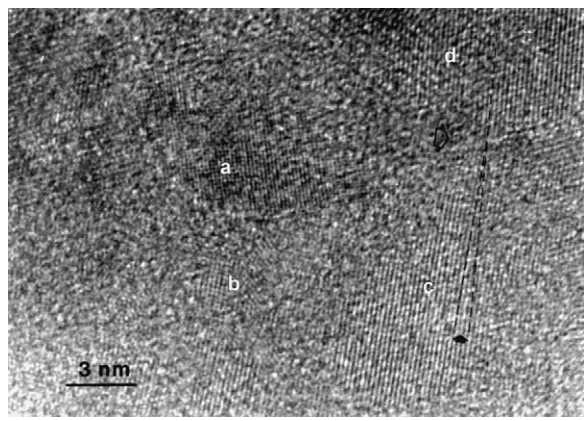

Fig. 13. A plane-view HRTEM image of the nanostructure in the top surface layer.

sized) were formed in the surface layer of the Fe sample during the SMA treatment. Based on the microstructure features observed in various sections with different strains in the deformed surface layer, one may find that the following elemental processes are involved in the grain refinement process:

1. development of DDWs and DTs in original grains and in the refined cells (under further straining) as well;
2. transformation of DDWs and DTs into subboundaries with small misorientations separating individual cells or subgrains;
3. evolution of subboundaries to highly misoriented grain boundaries.

The grain refinement mechanism can be schematically illustrated in Fig. 14, in which each process will be discussed in terms of the experimental observations.

4.1. Development of DDWs and DTs

In order to accommodate plastic strains in polycrystalline materials, various dislocation activities are normally motivated, including sliding, accumulation, interaction, tangling, and spatial rearrangement. In the SMA treated Fe sample, dislocation activities lead to formation of DDWs and DTs in original grains of the surface layer. Devel-

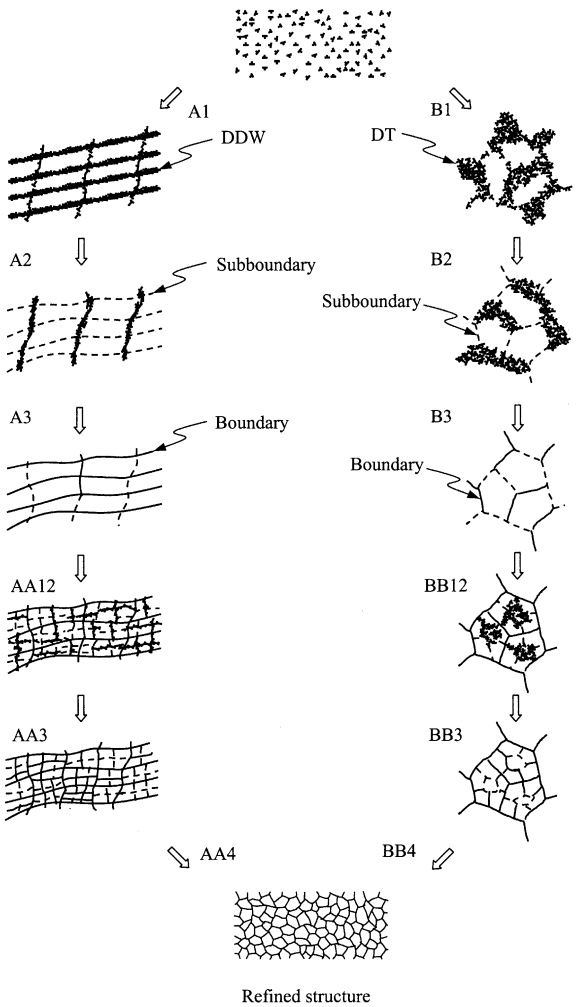

Fig. 14. A schematic illustration of grain refinement induced by plastic deformation.

opment of these dislocation configurations gradually results in subdivision of original grains by forming individual dislocation cells primarily separated by DDWs and DTs (Step A1 and B1 in Fig. 14), as can be clearly seen in Figs. 6–9 and in the literature as well [18,24]. The spacing of DDWs is directly related to the dislocation cell dimensions (L) formed in the coarse-grains, which are basically a function of the acting shear stress (τ) by $L = 10Gb/\tau$ with G being the shear modulus and b the Burgers vector [29]. Apparently, with an increasing shear stress, the lattice dislocation density increases, leading to smaller DDWs spacing and cell sizes.

The multi-directional peening in the SMA treatment may lead to the change of slip systems with the strain path even inside the same grain. The dislocations not only interact with other dislocations in the current active slip systems, but also interact with inactive dislocations generated in previous deformation. Therefore, the grains can be subdivided more efficiently by the DDWs and DTs in the SMA treatment with respect to other simple deformation techniques such as torsion and rolling.

4.2. Formation of subgrain boundaries

At a certain strain level, for minimizing the total system energy, dislocation annihilation and rearrangement occur in DDWs and DTs, which will transform into subboundaries (with increased misorientations relative to the DDWs) separating individual cells (Steps A2 and B2 in Fig. 14). Clearly, formation of subboundaries will reduce the density of lattice dislocations, and then the lattice microstrain will drop. Fig. 15 shows the variations of measured mean microstrain and average cell size in the surface layer (of about 5 μm deep) with the SMA treatment duration. The results show that during the initial stage of treatment, microstrain rapidly increases as the average cell size drastically decreases, implying multiplying of lattice dislocations and refinement of coarse grains.

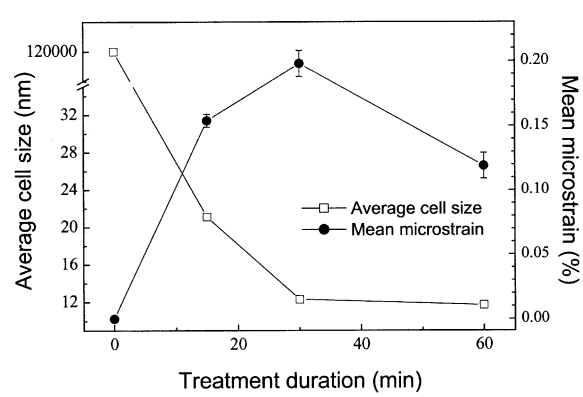

Fig. 15. Variations of the mean microstrain and the average cell size with the SMA treatment duration in the top surface layer of about 5 μm thick (determined by XRD experiments).

When the treatment duration exceeds 30 min, the cell size levels off but the microstrain drops from about 0.2 to 0.12%, indicating a significant annihilation of lattice dislocations due to formation of boundaries of subgrains (or grains) from DDWs.

4.3. Evolution of highly misoriented grain boundaries

With further increasing strains, the orientations of the grains with respect to their neighboring grains become completely random, and highly misoriented grain boundaries form (Step A3 and B3 in Fig. 14). The increment of misorientations between neighboring grains can be realized by accumulating and annihilating more dislocations in grain boundaries, or alternatively, by rotation of grains (or grain boundary sliding) with respect to each other under certain strains. The grain rotation process would be much facilitated when the size of grains is reduced due to the obvious size dependence [30].

With the further increase in strain, DDWs and DTs could form inside the inner of the refined subgrains and grains (Figs. 8 and 9), which indicates that the refined subgrains and grains could be subdivided following the similar mechanism (i.e. the path AA12 and BB12 to AA4 and BB4 in Fig. 14). With increasing strain, the subdivision takes place on a finer and finer scale. When dislocation multiplication rate is balanced by the annihilation rate, the increase of strains could not reduce the subgrain size any longer, and a stabilized grain size is resulted.

4.4. Formation of nanostuctures in the top surface layer

During the SMA treatment, the top surface layer is deformed at a very high strain rate. An estimated value of strain rate is about 10^3–10^4 s^{-1} in the top surface of the Fe sample, and it drops steeply with an increase of depth from the surface. Due to the high strain rate and the high strains, the deformed-induced dislocation density can be extremely high and DDWs with spacing in the nanometer regime will be formed. As can be seen in Figs. 11 and 12, lamellar dislocation cells and subgrains with nano-sized width are formed, which eventually transform into equiaxed nano-sized grains by development of DDWs and subgrain boundaries along the short axis (following A1–A3). Note that the grain rotation and grain boundary sliding will be much easier for nano-sized grains with respect to the coarse ones. Therefore, equiaxed nanocrystallites with random grain boundaries are readily formed (from A3–AA4) in the top surface layer, as always observed in the Fe sample treated by using SMA.

4.5. Effect of strain and strain rate

Based on the grain refinement mechanism discussed previously, one may find that strain and strain rate play an important role in the grain refinement process and the final stabilized grain size upon plastic deformation.

The effect of strain on the grain refinement has been demonstrated previously by numerous experiments. At a certain strain rate, an increase of strain leads to a higher density of dislocations and eventually to finer grains, which was observed in various deformed metals and alloys [31,32]. But the grain size could not be reduced infinitely, and a stabilized grain size (about 100–200 nm) is usually observed in many systems by means of ECAP and cold rolling [33,34]. In a recent work, nanostructures were produced by means of sliding deformation under large sliding loads [35]. The reason for obtaining the stabilized grain size with further straining might be that new DDWs and/or DTs could not be generated inside the refined grains due to the balance between dislocation multiplication and annihilation at the certain strain rate.

Experiments showed that nanocrystallites with grain size of about 10 nm can be obtained during ball-milling [32] and SMA treatment of metals [13], in which much larger strain rates (with comparable strains) are applied compared to those in the ECAP and the rolling processes. It is known that at a given level of strain, dislocation density increases with an increasing strain rate. The much larger strain rate in the ball-milling and SMA process may produce a much larger dislocation density in the sample, resulting in formation of more DDWs and DTs with smaller sized cells, and eventually forming finer grains. There are also evi-

dences showing that higher strain rates raise the misorientation across adjacent substructures up to a higher value than lower strain rate [36].

In addition, it should be mentioned that temperature plays a role in the grain refinement, as the dislocation activity is sensitive to temperature. The dislocation activities will be depressed at lower temperatures, and therefore, finer grains are expected to be obtained in plastic deformation at lower temperatures. More systematic experimental investigations are needed to demonstrate this effect.

5. Summary

Nanocrystalline structure was obtained in the surface layer of a pure Fe plate subjected to SMA treatments. Based on the microstructure observations, a grain refinement mechanism induced by plastic deformation during SMA treatment in Fe is proposed. It involves formation of DDWs and DTs in original grains and in the refined cells (under further straining) as well, transformation of DDWs and DTs into subboundaries with small misorientations separating individual cells or subgrains, and evolution of subboundaries to highly misoriented grain boundaries. Experimental evidences and analysis of the grain refinement mechanism indicate that high strains with a high strain rate are necessary for formation of nanocrystallites during plastic deformation of metals.

6. Acknowledgments

Financial support from the National Science Foundation of China, the Ministry of Science and Technology of China (Grant G1999064505), NEDO International Joint Research Grant Program (01MB5), and Ministry of Research of France (Grant 2001882, CPER EN2040) is acknowledged. The authors thank Prof. N. Hansen for his stimulating discussions.

References

[1] Cahn RW. Nature 1990;348:389.
[2] Bohn R, Haubopld T, Birringer R, Gleiter H. Scr Metall Mater 1991;25:811.
[3] Tang JSC, Koch CC. Scr Metall Mater 1990;24:1599.
[4] Morris DG. In: Mechanical behavior of nanostuctured materials. Clausthal, Germany: Trans. Tech. Publications Ltd; 1998. p. 70.
[5] Mcfadden SX, Mishra RS, Valiev RZ, Zhilyaev AP, Mukherjee AK. Nature 1999;398:684.
[6] Lu L, Sui ML, Lu K. Science 2000;287:1463.
[7] Birringer R, Gleiter H, Klein HP, Marquardt P. Phys Lett 1984;102A:365.
[8] Lu K, Wang JT, Wei WD. J Appl Phys 1991;69:522.
[9] Koch CC. Mater Sci Forum 1992;88-90:243.
[10] Valiev RZ, Korznikov AV, Mulyukov RR. Mater Sci Eng 1993;A168:141.
[11] Erb U, EI-Sherik AM, Palumbo G, Aust KT. Nonostruct Mater 1993;2:383.
[12] Lu K, Lu J. J Mater Sci Technol 1999;15:193.
[13] Tao NR, Sui ML, Lu J, Lu K. Nanostruct Mater 1999;11:433.
[14] Liu G, Lu J, Lu K. Mater Sci Eng 2000;A286:91.
[15] Lu K, Lu J. Chinese Patent, No. 01122980, 2 (2001); French Patent, FR2812284 (2001).
[16] Lasalmoni A, Stryel JL. J Mater Sci 1986;21:1837.
[17] Zhilyaev AP, Lee S, Nurislamova GV, Valiev RZ, Langdon TG. Scr Mater 2001;44:2753.
[18] Bay B, Hansen N, Hughes DA, Kuhlmann-Wilsdorf D. Acta Metall Mater 1992;40:205.
[19] Horita Z, Smith DJ, Nemoto M, Valiev RZ, Langdon TG. J Mater Res 1998;13:446.
[20] Fecht HJ. In: Hadjipanayis GC, Siegel RW, editors. Nanophase materials. The Netherlands: Kluwer Academic Publishers; 1994. p. 125.
[21] Koch CC. Nanostruct Mater 1993;2:109.
[22] Eckert J, Holzer JC, Johnson WL. Scr Metall Mater 1992;27:1105.
[23] Klug HP, Alexander LE. In: X-ray diffraction procedures for polycrystalline and amorphous materials. New York: Wiley; 1974. p. 661.
[24] Hansen N. Mater Sci Tech 1990;6:1039.
[25] Moelle CH, Fecht HJ. Nanostruct Mater 1995;6:421.
[26] Langford G, Cohen M. Trans ASM 1969;82:623.
[27] Jago RA, Hansen N. Acta Metall 1986;34:1711.
[28] Valiev RZ, Islamgaliev RK, Alexandrov IV. Prog Mater Sci 2000;45:103.
[29] Kuhlmann-Wilsdorf D, Van der Merwe JH. Mater Sci Eng 1982;55:79.
[30] Von Swygenhoven H, Farkas D, Caro A. Phys Rev B 2000;62:831.
[31] Iwahashi Y, Horita Z, Nemoto M, Landon TG. Acta Metall 1998;46:3317.
[32] Malow TR, Koch CC. Metall Mater Trans A 1998;29:2285.

[33] Shin DH, Kim I, Kim J, Park K. Acta Metall 2001;49:1285.
[34] Gholinia A, Prangnell PB, Markushev MV. Acta Metall 2000;48:1115.
[35] Hughes DA, Hansen N. Phys Rev Lett 2001;87:135503-1.
[36] Hines JA, Vecchio KS, Ahzi S. Metall Mater Trans A 1998;29:191.